

Article

# Microwave-Assisted Synthesis of $\text{Co}_3(\text{PO}_4)_2$ Nanospheres for Electrocatalytic Oxidation of Methanol in Alkaline Media

Prabhakarn Arunachalam \*, Maged N. Shaddad, Abdullah Salah Alamoudi, Mohamed A. Ghanem and Abdullah M. Al-Mayouf

Electrochemistry Research Group, Chemistry Department, College of Science, King Saud University, Riyadh 11451, Saudi Arabia; mshadad@ksu.edu.sa (M.N.S.); Abdullahamoudi8@icloud.com (A.S.A.); mghanem@ksu.edu.sa (M.A.G.); amayouf@ksu.edu.sa (A.M.A.-M.)

\* Correspondence: parunachalam@ksu.edu.sa or prabhuchemist@hotmail.com; Tel.: +966-114696026

Academic Editor: Giancarlo Cravotto

Received: 16 January 2017; Accepted: 12 April 2017; Published: 17 April 2017

**Abstract:** Low-cost and high-performance advanced electrocatalysts for direct methanol fuel cells are of key significance for the improvement of environmentally-pleasant energy technologies. Herein, we report the facile synthesis of cobalt phosphate ( $\text{Co}_3(\text{PO}_4)_2$ ) nanospheres by a microwave-assisted process and utilized as an electrocatalyst for methanol oxidation. The phase formation, morphological surface structure, elemental composition, and textural properties of the synthesized ( $\text{Co}_3(\text{PO}_4)_2$ ) nanospheres have been examined by powder X-ray diffraction (XRD), Fourier transform-infrared spectroscopy (FT-IR), field emission-scanning electron microscopy (FE-SEM), high-resolution transmission electron microscopy (HRTEM), X-ray photoelectron spectroscopy (XPS), and nitrogen adsorption-desorption isotherm investigations. The performance of an electrocatalytic oxidation of methanol over a  $\text{Co}_3(\text{PO}_4)_2$  nanosphere-modified electrode was evaluated in an alkaline solution using cyclic voltammetry (CV) and chronopotentiometry (CP) techniques. Detailed studies were made for the methanol oxidation by varying the experimental parameters, such as catalyst loading, methanol concentration, and long-term stability for the electro-oxidation of methanol. The good electrocatalytic performances of  $\text{Co}_3(\text{PO}_4)_2$  should be related to its good surface morphological structure and high number of active surface sites. The present investigation illustrates the promising application of  $\text{Co}_3(\text{PO}_4)_2$  nanospheres as a low-cost and more abundant electrocatalyst for direct methanol fuel cells.

**Keywords:** cobalt phosphate; direct methanol fuel cell; electrocatalysts; methanol; microwave-assisted synthesis; oxidation

## 1. Introduction

Concerns of the expanding demand for energy by humankind and the quick consumption of fossil fuels have set off the need to plan and create novel advances for the production of energy in a sustainable way [1,2]. Direct alcohol fuel cells (DAFCs) have engrossed significant interest as a power source for handy applications, such as laptops, mobile phones, automobiles, and digital cameras, etc. [3]. The concerns with storage and transport of alcohols (such as ethanol, methanol, glycerol, and ethylene glycol) are more user-responsive compared to hydrogen [4]. The most frequent DAFC is the direct methanol fuel cell (DMFC), which relies upon the oxidation of methanol over the surface of the catalysts. In recent years, DMFCs are considered as one of the most promising candidate for solving the energy crisis because of their high energy conversion efficiency, non-toxic nature, less noise, and low operating temperature [5,6]. Electrocatalytic oxidation of methanol is the prime step in

the progress of DMFCs. Conventionally, platinum and platinum-based alloys are extensively used as promising electrocatalysts for the oxidation of alcohols due to their outstanding electrocatalytic activities. However, what strongly limit their large-scale applications are the expensive noble metals and their lower abundance in nature. This concern has brought more attention on researchers to develop an alternative low-cost and high catalytic performance for the electrocatalytic oxidation of alcohols.

Over the past few years, several other functional electrocatalytic materials have been engaged as alternatives to noble Pt electrocatalysts in DMFCs which consist of metal oxides [7,8], carbonaceous materials [9,10], metal chalcogenides [11–13], and phosphates [14,15]. More recently, metal phosphates have exposed as an efficient electrocatalysts for the uses in various applications due to their exclusive physical and chemical properties. Many researchers have examined Co-based electrocatalysts for the oxidation of alcohols and energy-related applications [16–24]. Due to the mesoporous-structured nature, highly active surface area, non-toxic nature, and greater abundance of Co-based electrocatalyst show an enhanced property for several applications.

Herein, we report a microwave-assisted process for the fabrication of porous  $\text{Co}_3(\text{PO}_4)_2$  nanospheres. In this work, we have used a microwave-assisted process in order to avoid particle aggregation during the precipitation of  $\text{Co}_3(\text{PO}_4)_2$  nanospheres and an arrangement of good morphological features. The good surface morphological features of the catalyst are always desired to improve the electrocatalytic performance. The electrocatalytic activity of the synthesized  $\text{Co}_3(\text{PO}_4)_2$  nanospheres was examined by the electrocatalytic methanol oxidation. The crystallinity, purity of phase, textural properties, and electrochemical performances of synthesized  $\text{Co}_3(\text{PO}_4)_2$  were examined by powder X-ray diffraction (XRD), Fourier transform-infrared spectroscopy (FT-IR), X-ray photoelectron spectroscopy (XPS), Brunauer–Emmett–Teller (BET), and electrochemical (voltammetric) measurements.

## 2. Results and Discussion

### 2.1. Powder XRD Analysis

The crystallinity and phase formation of the  $\text{Co}_3(\text{PO}_4)_2$  materials was examined by powder XRD analysis and the resulting XRD pattern is presented in Figure 1. The diffraction peaks of the calcined  $\text{Co}_3(\text{PO}_4)_2$  at 600 °C (Figure 1d) showed numerous peaks which are consistent with the diffraction planes. The detected (hkl) planes are indexed, agreeing with the stated hexagonal phase of  $\text{Co}_3(\text{PO}_4)_2$  (JCPDS No. 70–1795, Figure 1a). Conversely, it is observed that the XRD pattern of the as-synthesized (Figure 1b) and calcined  $\text{Co}_3(\text{PO}_4)_2$  at 300 °C (Figure 1c) showed two broad humps at a  $2\theta$  value of 35° and 55° (Figure 1c). This broad peak established that the  $\text{Co}_3(\text{PO}_4)_2$  showed an amorphous nature [19,20]. The calcined  $\text{Co}_3(\text{PO}_4)_2$  at 600 °C sample shows the strong crystalline nature of  $\text{Co}_3(\text{PO}_4)_2$  compared to others. We have also measured the average crystalline size, which was observed to be 32.07 nm for calcined  $\text{Co}_3(\text{PO}_4)_2$ .

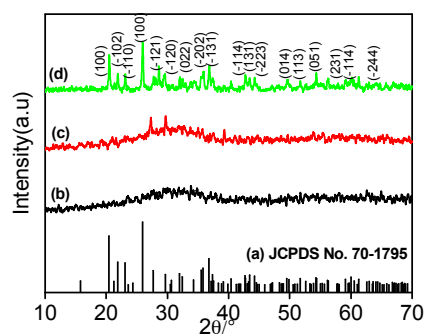


**Figure 1.** The powder X-ray diffraction (XRD) pattern of the (a) hexagonal  $\text{Co}_3(\text{PO}_4)_2$ —JCPDS No. 70-1795; (b) as-synthesized, calcined  $\text{Co}_3(\text{PO}_4)_2$  at (c) 300 °C; and (d) 600 °C.

## 2.2. FT-IR Spectroscopy Analysis

The chemical interactions occurred in  $\text{Co}_3(\text{PO}_4)_2$  nanospheres were examined by FT-IR spectroscopy. The FT-IR spectra of  $\text{Co}_3(\text{PO}_4)_2$  was evident in the region of  $500\text{--}4000\text{ cm}^{-1}$  and the experimental spectrum is shown in Figure 2. In the  $\text{Co}_3(\text{PO}_4)_2$  spectrum, the vibrational band at  $689\text{ cm}^{-1}$  is ascribed to the  $\text{V}_4(\text{F}_2)\text{PO}_4^{3-}$  mode of the phosphate ( $\text{PO}_4$ ) group [25]. The broad characteristic peaks at  $1017$  and  $1365\text{ cm}^{-1}$  are attributed to the survival of the P=O stretching vibration in  $\text{PO}_4^{3-}$  and the P–O–P stretching vibration in the  $\text{HPO}_4^{2-}$  group, respectively [26]. The distinguished broad vibration peak at  $3425\text{ cm}^{-1}$  is assigned to the stretching frequency of the O–H group. The FT-IR results distinctly suggested the subsistence of the  $\text{Co}_3(\text{PO}_4)_2$  sample.

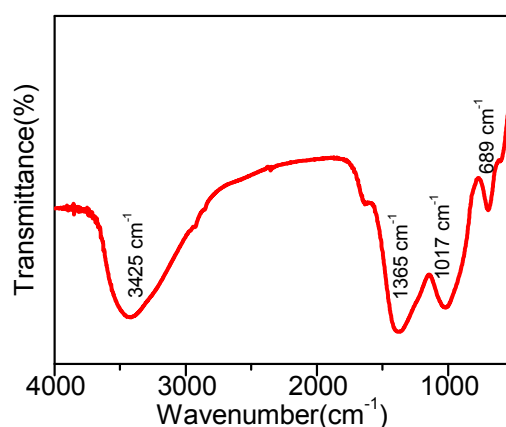


**Figure 2.** The FT-IR spectrum of  $\text{Co}_3(\text{PO}_4)_2$  nanospheres.

## 2.3. Morphological Analysis

The surface morphology of the porous  $\text{Co}_3(\text{PO}_4)_2$  materials were analyzed by FE-SEM and the resultant images are displayed in Figure 3a,b. FE-SEM results of  $\text{Co}_3(\text{PO}_4)_2$  show nanosphere like morphology and form a hierarchical nanostructure with uniformly-packed  $\text{Co}_3(\text{PO}_4)_2$  with an average size of  $\sim 100$  to  $200\text{ nm}$ . It can be noticed that the surface morphology of the  $\text{Co}_3(\text{PO}_4)_2$  sample are tightly-packed nanosphere-like particles which can offer support for effective electron transport [27]. Further in-depth exploration on the surface morphology of  $\text{Co}_3(\text{PO}_4)_2$  samples was observed by HRTEM and the equivalent images are shown in Figure 4a,b. The HRTEM images also confirmed the nanosphere-like surface morphology of  $\text{Co}_3(\text{PO}_4)_2$  samples having an average particle size of  $\sim 100\text{ nm}$ .

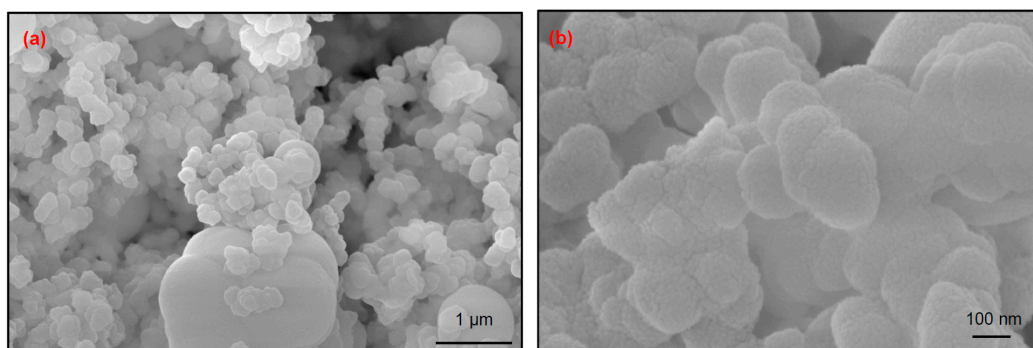


**Figure 3.** Field emission-scanning electron microscopy (FE-SEM) images (a) high- and (b) low-scale magnification image of a synthesized  $\text{Co}_3(\text{PO}_4)_2$  nanosphere sample.

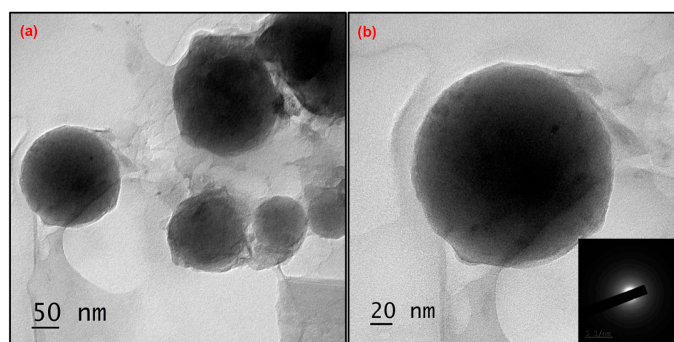


**Figure 4.** (a,b) High-resolution transmission electron microscopy (HRTEM) image of the  $\text{Co}_3(\text{PO}_4)_2$  nanosphere sample calcined at 300 °C.

#### 2.4. XPS Analysis

The elemental compositions and chemical bonding of the synthesized  $\text{Co}_3(\text{PO}_4)_2$  nanospheres was investigated by XPS. The survey spectra of  $\text{Co}_3(\text{PO}_4)_2$  (Figure 5a) clearly evidenced the presence of Co, P, and O elements in the synthesized  $\text{Co}_3(\text{PO}_4)_2$  sample. The high-resolution XPS spectra for  $\text{Co}_{2p}$ ,  $\text{P}_{2p}$ , and  $\text{O}_{1s}$  species are presented in Figure 5b–d. The binding energy of  $\text{Co}_{2p}$  (Figure 5b) appeared in two peaks around 782 and 798 eV, which are ascribed to  $\text{Co}_{2p_{3/2}}$  and  $\text{Co}_{2p_{1/2}}$ , respectively and also with two shake-up satellites. Figure 5c demonstrated the binding energy of  $\text{P}_{2p}$  which is centered at 134 eV. The peaks centered at 133.4, 134.1, and 135.2 eV related to the characteristics peaks of P(V) of the  $\text{Co}_3(\text{PO}_4)_2$  sample (Figure 5c). The observed binding energy around 532 eV of  $\text{O}_{1s}$  is attributed to the bonding of metal oxide (Figure 5d). The fitted peak at 531.6 can related to the metal-oxygen bonds and the peak at 532.6 eV related to the oxygen of OH groups. Further, the peak at 533.9 can be related to the adsorbed water near the surface. (Figure 5d). The examined XPS analysis clearly demonstrated the formation of  $\text{Co}_3(\text{PO}_4)_2$  materials and the obtained results are consistent with powder XRD analysis.

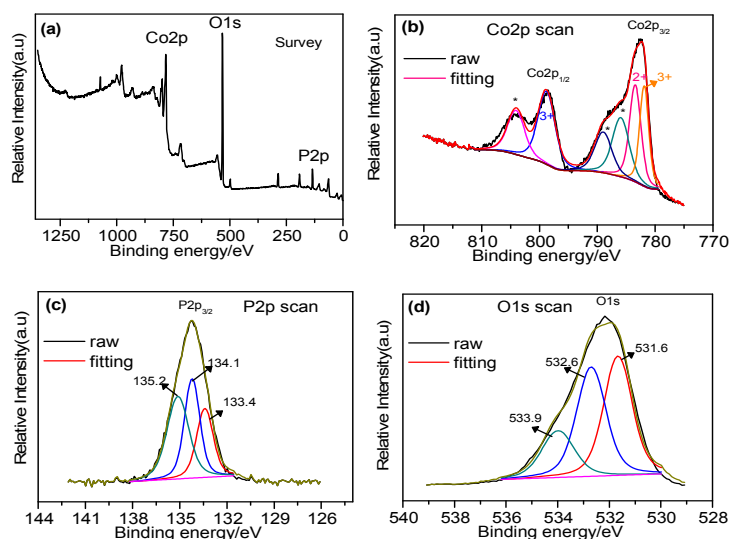


**Figure 5.** (a) X-ray photoelectron spectroscopy (XPS) survey spectrum of  $\text{Co}_3(\text{PO}_4)_2$  nanospheres, (b)  $\text{Co}_{2p}$ , (c)  $\text{P}_{2p}$ , and (d)  $\text{O}_{1s}$  spectra of  $\text{Co}_3(\text{PO}_4)_2$  nanospheres. (\* indicates satellite peak).

#### 2.5. Textural Properties

The nitrogen adsorption-desorption isotherm analysis was carried out to examine the textural properties, such as BET surface area, pore size, and pore volume of the synthesized  $\text{Co}_3(\text{PO}_4)_2$

nanospheres. The adsorption–desorption isotherms of  $\text{Co}_3(\text{PO}_4)_2$  nanospheres are displayed in Figure 6. Based on IUPAC classification, the isotherm of  $\text{Co}_3(\text{PO}_4)_2$  nanospheres exposes a type IV isotherm with distinct H3 hysteresis loops in a  $P/P_0$  range of 0.1 to 1, which is related to the porous materials. The examined specific BET surface area value from adsorption-desorption isotherms was  $20.2 \text{ m}^2/\text{g}$ . In addition, Figure 6 (inset) demonstrates the BJH pore size distribution of  $\text{Co}_3(\text{PO}_4)_2$  nanospheres with average pore size and volume around  $0.98 \text{ nm}$  and  $1.001 \times 10^{-2} \text{ mL/g}$ , respectively. It can be noted that the good surface morphology and textural properties are benefits for the enhancement of electrode/electrolyte interfacial area, which can improve the electrocatalytic active sites for electrocatalytic oxidation of methanol.

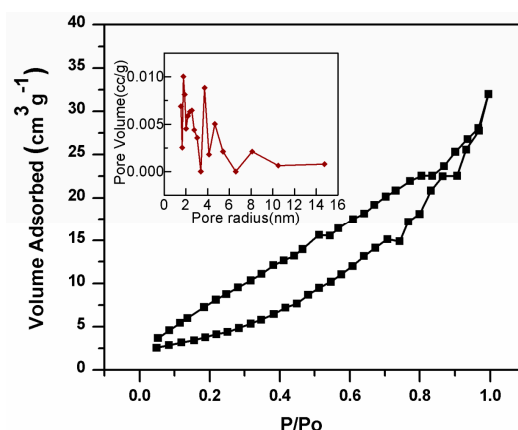


**Figure 6.**  $\text{N}_2$  adsorption-desorption isotherms of  $\text{Co}_3(\text{PO}_4)_2$  nanospheres. The inset of Figure 6 shows the pore size distribution.

## 2.6. Electrocatalytic Methanol Oxidation over $\text{Co}_3(\text{PO}_4)_2$ Nanospheres

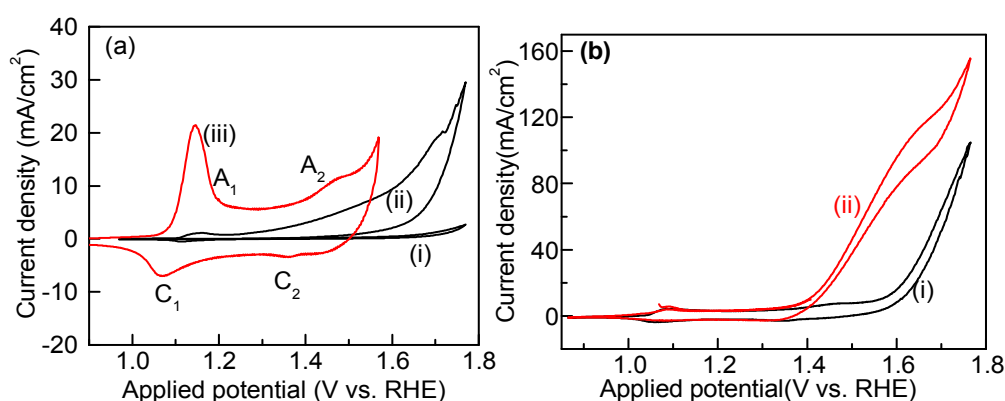
The electrochemical performances of the  $\text{Co}_3(\text{PO}_4)_2$  nanosphere catalyst, with regard to oxidation-reduction reactions in alkaline media, were evaluated and compared with bulk  $\text{Co}_3(\text{PO}_4)_2$  fabricated in the absence of any reducing agent. Figure 7a displays the cyclic voltammetry at  $50 \text{ mV}\cdot\text{s}^{-1}$  in  $1.0 \text{ M KOH}$  solution for loaded catalysts on an Au electrode. The cyclic voltammograms (CV) show two redox peaks ( $A_1/C_1 = \text{Co}^{2+}/\text{Co}^{3+}$ ) and ( $A_2/C_2 = \text{Co}^{3+}/\text{Co}^{4+}$ ) located at about  $1.12/1.08$  and  $1.45/1.38 \text{ V vs. RHE}$ , respectively, for  $\text{Co}_3(\text{PO}_4)_2$  nanospheres and are typically similar to those reported in the literature [28]. The CV curves of  $\text{Co}_3(\text{PO}_4)_2$ -modified electrode (Figure 7a) exhibit a redox peak prior to the oxygen evolution reactions can be credited to the well-known redox reaction of  $\text{Co(II)}/\text{Co(III)}$  and a feasible electrochemical reaction in a  $\text{KOH}$  solution is afforded in reaction (1):



It is evidenced that the redox peak currents of  $\text{Co}_3(\text{PO}_4)_2$  nanosphere catalyst voltammograms are significantly higher (15 times) than the current for bulk  $\text{Co}_3(\text{PO}_4)_2$  signifying substantially higher electrochemical area and higher capacitance current for  $\text{Co}_3(\text{PO}_4)_2$  nanosphere catalysts.

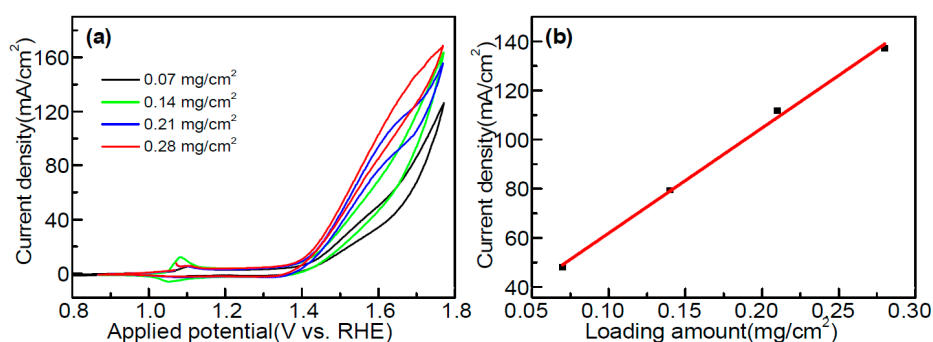
The profile of CVs of the  $\text{Co}_3(\text{PO}_4)_2$ -modified electrode at a scan speed of  $50 \text{ mV}\cdot\text{s}^{-1}$  in  $1.0 \text{ M KOH}$  solution with and without the presence of  $1.0 \text{ M}$  methanol is exhibited in Figure 7b. Prior to examining the electrocatalytic methanol oxidation activity of  $\text{Co}_3(\text{PO}_4)_2$  nanospheres, the electrochemical properties of the  $\text{Co}_3(\text{PO}_4)_2$  nanosphere-modified electrode was scrutinized in  $1.0 \text{ M KOH}$  solution. The CV of the  $\text{Co}_3(\text{PO}_4)_2$ -modified electrode (Figure 7b) in  $1.0 \text{ M KOH} + 1.0 \text{ M CH}_3\text{OH}$  shows a considerable increment in the oxidation peak current density at an oxidation peak potential of  $1.65 \text{ V}$  (vs. RHE) and also noticed that the decrease in the redox peak during the reverse scan. In addition, the methanol catalytic oxidation current tends to increase with the positive scan until reaching a plateau of about  $120 \text{ mA}/\text{cm}^2$  at  $1.7 \text{ V}$  vs. RHE. Moreover, it is observed that the oxygen evolution reaction

occurs at more positive potentials in the presence of methanol solutions which can be clarified by the greater affinity of  $\text{Co}^{3+}$  intermediate species ( $\text{CoOOH}$ ) to adsorb methanol than to  $\text{OH}^-$  ions [29]. Thus, the increased oxidation current and the departed redox peak in the presence of  $\text{CH}_3\text{OH}$  in  $\text{KOH}$ , when compared to pure  $\text{KOH}$  solution, revealed the electrocatalytic activity of  $\text{Co}_3(\text{PO}_4)_2$  for the oxidation of methanol. The electrocatalytic performances of  $\text{Co}_3(\text{PO}_4)_2$  are nearly related to its good surface morphology and high active surface area, which was completely investigated with the results obtained above in FE-SEM, HRTEM, and BET analysis.



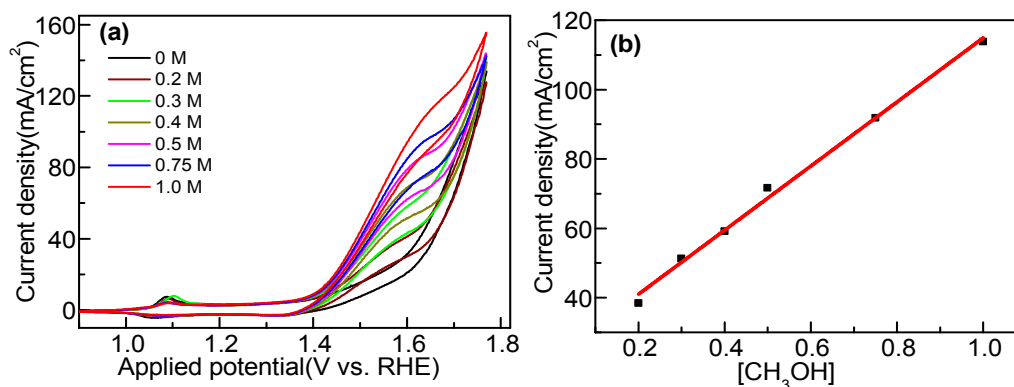
**Figure 7.** Cyclic voltammograms (CV) of 50 mV/s in 1.0 M  $\text{KOH}$  solution for  $2.1 \text{ g/cm}^2$  for (a): blank (i) bulk- $\text{Co}_3(\text{PO}_4)_2$  (ii) and  $\text{Co}_3(\text{PO}_4)_2$  nanospheres (iii) loaded on an Au electrode; (b) CVs of  $\text{Co}_3(\text{PO}_4)_2$  nanosphere-modified electrode at 50 mV/s in 1.0 M  $\text{KOH}$  for (i) in absence, and (ii) in presence of 1.0 M  $\text{CH}_3\text{OH}$ .

We have examined the effect of the catalyst loading amount on the electrocatalytic oxidation of methanol in 1.0 M  $\text{KOH} + 1.0 \text{ M CH}_3\text{OH}$  and the corresponding CV profile is shown in Figure 8a. It can be seen that the methanol oxidation current is noticeably enhanced. Figure 8b shows the plot of anodic methanol oxidation current density vs. electrocatalyst loading amount at 1.65 V vs. RHE, and this clearly reveals that the linear increase of the oxidation current with a catalyst loading amount ( $0.07$  to  $0.28 \text{ mg/cm}^2$ ) may be due to an increase in the number of accessible active catalyst sites and efficient mass transport ions into the  $\text{Co}_3(\text{PO}_4)_2$  catalyst [29]. Additionally, it can be seen that the oxidation potential is shifted towards the negative potential when the electrocatalyst loading amount increased, which suggests good kinetic performance for the oxidation of methanol.



**Figure 8.** CVs of  $\text{Co}_3(\text{PO}_4)_2$  nanosphere-modified electrode at 50 mV/s (a) at various  $\text{Co}_3(\text{PO}_4)_2$  loadings, and (b) the plot of anodic methanol oxidation current density vs. the electrocatalyst loading amount at 1.65 V vs. RHE.

The CVs at 50 mV/s for 0.28 mg/cm<sup>2</sup> loaded Co<sub>3</sub>(PO<sub>4</sub>)<sub>2</sub> nanospheres in various concentrations of CH<sub>3</sub>OH solution are presented in Figure 9a. It can be observed that the CH<sub>3</sub>OH oxidation peak current density gradually increases with a shifting of the peak potential towards the positive potential as the concentration of methanol increases (Figure 9a). The linear relationship between the methanol concentration and the oxidation peak current at 1.65 V vs. RHE is plotted and shown in Figure 9b. This clearly showed the increase of methanol oxidation current linearly with the concentration of the methanol solution, which illustrates that Co<sub>3</sub>(PO<sub>4</sub>)<sub>2</sub> nanospheres have good tolerance for product adsorption [29].

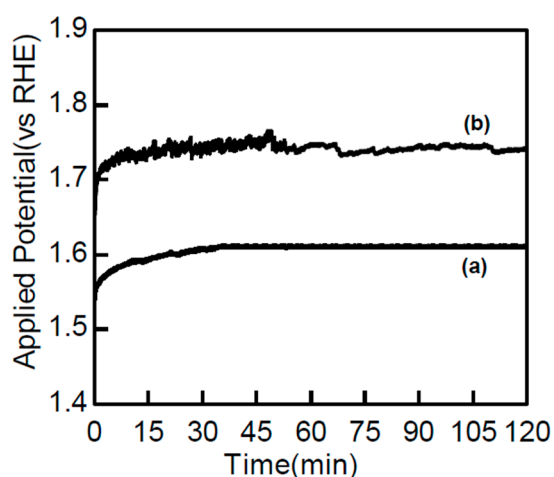


**Figure 9.** CVs of a Co<sub>3</sub>(PO<sub>4</sub>)<sub>2</sub> nanosphere-modified electrode at 50 mV/s, (a) under various concentration of methanol solution, and (b) the plot of anodic methanol oxidation current density vs. methanol concentration at 1.65 V vs. RHE.

The electrochemical long-term stability of the Co<sub>3</sub>(PO<sub>4</sub>)<sub>2</sub> nanosphere-modified electrode is also an important factor for the electro-oxidation of methanol. The long-term stability was examined using chronopotentiometry measurements at two different current densities (25 and 75 mA/cm<sup>2</sup>) in 0.14 mg/cm<sup>2</sup> loaded Co<sub>3</sub>(PO<sub>4</sub>)<sub>2</sub> nanospheres and the obtained result is shown in Figure 10. It can be seen from Figure 10 that the Co<sub>3</sub>(PO<sub>4</sub>)<sub>2</sub> nanosphere-modified electrode demonstrated nearly constant operating potentials at 1.53 and 1.73 V vs. RHE for 25 and 75 mA/cm<sup>2</sup> during 120 min of methanol oxidation testing. This suggests that Co<sub>3</sub>(PO<sub>4</sub>)<sub>2</sub> nanospheres are relatively stable and tolerant of high poisoning levels for the oxidation of methanol. At the start of the reaction, the operating potentials are shown gradually increasing and reach steady-state which indicates incompletely-adsorbed oxidation products for a few minutes, initially. Table 1 displays the specific mass activities of nickel- and cobalt-based catalyst for methanol electro-oxidation, and it is evidenced that the methanol electro-oxidation catalytic steady-state specific activities of the Co<sub>3</sub>(PO<sub>4</sub>)<sub>2</sub> nanosphere catalyst is superior than other nickel- and cobalt-based catalysts. The electrostability of the Co<sub>3</sub>(PO<sub>4</sub>)<sub>2</sub> electrocatalyst also confirmed the feasible application of Co<sub>3</sub>(PO<sub>4</sub>)<sub>2</sub> nanospheres as a capable low-cost substitute to Pt-based electrocatalysts for methanol oxidation. Lastly, and in comparison with other nickel- and cobalt-based catalysts, it is found that the methanol oxidation is significantly higher than that for cobalt-based catalysts. However, detailed study needs to be carried out to establish the Co<sub>3</sub>(PO<sub>4</sub>)<sub>2</sub> nanosphere-based electrocatalyst to be more competitive for the methanol electro-oxidation reaction.

**Table 1.** Specific and mass activities of nickel- and cobalt-based catalysts for methanol oxidation in alkaline media.

Sr. No.	Catalyst	Method	Electrolyte (M)	Current Density mA mg <sup>-1</sup> /mA cm <sup>-2</sup>	Ref.
1	Ni-Cu-P/C	Electroless deposition	KOH: 0.1 CH <sub>3</sub> OH: 0.5	-/9.5	[30]
2	Pt/C	Chemical reduction	KOH: 1 CH <sub>3</sub> OH: 1	-/40	[31]
3	Pd/C	Hydrothermal	KOH: 1 CH <sub>3</sub> OH: 1	-/24	[31]
4	NiO/MWCNT	Pulsed Electrodeposition	NaOH: 0.1 CH <sub>3</sub> OH: 0.1	-/10	[32]
5	Co-Cu-CNF	Electrospinning	KOH: 1 CH <sub>3</sub> OH: 2	-/16	[33]
6	Pt/Ni(OH) <sub>2</sub> /Graphene	Two-step solution method	KOH: 0.1 CH <sub>3</sub> OH: 0.5	400/-	[34]
7	Co <sub>3</sub> O <sub>4</sub>	Microwave	KOH: 1 CH <sub>3</sub> OH: 1	335/75	[28]
8	Co <sub>3</sub> (PO <sub>4</sub> ) <sub>2</sub> nanospheres	Microwave	KOH: 1 CH <sub>3</sub> OH: 1	556/126	This work

**Figure 10.** Chronopotentiometry curves of methanol oxidation over a Co<sub>3</sub>(PO<sub>4</sub>)<sub>2</sub> nanosphere-modified electrode under constant current densities of 25 (a) and 75 mA/cm<sup>2</sup> (b).

### 3. Experimental

#### 3.1. Microwave-Assisted Synthesis of Co<sub>3</sub>(PO<sub>4</sub>)<sub>2</sub> Nanospheres

The porous Co<sub>3</sub>(PO<sub>4</sub>)<sub>2</sub> nanospheres were synthesized through a microwave-assisted process using cobalt nitrate (Co(NO<sub>3</sub>)<sub>2</sub>·6H<sub>2</sub>O; Sigma Aldrich, St. Louis, MO, USA) and di-sodium hydrogen phosphate (Na<sub>2</sub>HPO<sub>4</sub>; Sigma Aldrich) as the cobalt and phosphate sources, respectively. For instance, the evaluated amount of Co(NO<sub>3</sub>)<sub>2</sub>·6H<sub>2</sub>O (0.2 M) and Na<sub>2</sub>HPO<sub>4</sub> (0.2 M) was dissolved along with 0.8 M of urea (NH<sub>2</sub>CONH<sub>2</sub>; Sigma Aldrich) in 40 mL of deionized water under ultrasonication for 30 min. Concisely, the amount of cobalt phosphate precursor and urea with a molar ratio of 1:4 were dissolved in 40 mL of water to obtain a homogenous solution. Then, 90 mL of ethylene glycol was added under ultrasonic agitation until the homogenous reaction mixture was obtained. The acquired homogenous solution was placed in a microwave oven and the microwave reaction was carried out under 600 W microwave irradiation for 15 min to form Co<sub>3</sub>(PO<sub>4</sub>)<sub>2</sub> products. The obtained precipitate after filtration was processed via several washings with deionized water, absolute ethanol, and dried

at 80 °C for 3 h. Finally, the obtained  $\text{Co}_3(\text{PO}_4)_2$  product was annealed for 1 h at 300 and 600 °C. For comparison purposes, the bulk  $\text{Co}_3(\text{PO}_4)_2$  particles were obtained and prepared without any reducing agent.

### 3.2. Instrumental Characterization

The crystallinity and phase formation of the synthesized  $\text{Co}_3(\text{PO}_4)_2$  sample was analyzed by powder XRD (Rigaku Miniflex 600, Rigaku corporation, Tokyo, Japan) with copper  $\text{K}\alpha$  radiation ( $\lambda = 1.5418 \text{ \AA}$ ) at a scan speed of  $3^\circ/\text{min}$ . The chemical interactions that occurred in  $\text{Co}_3(\text{PO}_4)_2$  were examined using FT-IR spectroscopy (FT-IR, Thermofisher Scientific, Waltham, MA, USA). The surface morphology of the  $\text{Co}_3(\text{PO}_4)_2$  materials were examined by FE-SEM (SEM, JSM-6380, JEOL, Peabody, MA, USA) and HRTEM (TEM, JEOL). The elemental compositions and chemical bonding of the synthesized  $\text{Co}_3(\text{PO}_4)_2$  nanospheres JEOL-6330, USA were investigated by XPS (XPS, Thermo Scientific). The textural properties of the BET surface area, pore size, and pore volume were assessed on the basis of nitrogen adsorption-desorption isotherms using a NOVA 2200e analyser (Quantachrome Instruments, Boynton Beach, FL, USA).

### 3.3. Electrochemical Analysis

All of the electrochemical analyses were conducted in a conventional three-electrode system using a potentiostat (VSP-0478, Biologic, Seyssinet-Pariset, France, with ECLAB software, 10.1, Biologic, Seyssinet-Pariset, France, 2011) in a 1.0 M KOH (pH = 13) solution. The electrodes consisted of Pt foil, a saturated calomel electrode, and a  $\text{Co}_3(\text{PO}_4)_2$  electrocatalyst ink drop-casted Au electrode as the counter, reference, and working electrodes, respectively. The  $\text{Co}_3(\text{PO}_4)_2$  electrocatalyst ink was prepared by dispersion of a fixed amount of the  $\text{Co}_3(\text{PO}_4)_2$  electrocatalyst dispersed in 0.4 mL of 2-propanol, 0.1 mL of water, and 40  $\mu\text{L}$  of 5 wt % Nafion under ultrasonication. The obtained electrocatalyst ink (0.07 to 0.28  $\text{mg}/\text{cm}^2$ ) was drop-casted on the Au electrode and left in air to dry for approximately 1 h.

## 4. Conclusions

In summary, we successfully demonstrated a facile synthesis of  $\text{Co}_3(\text{PO}_4)_2$  nanospheres by a microwave-assisted method and utilized as an electrocatalyst for the oxidation of methanol. The phase formation, morphological surface structure, elemental composition and textural properties of the sample was examined by various physicochemical characterization methods, such as powder XRD, FT-IR, FE-SEM, HRTEM, XPS, and BET surface analyses. The detailed electrochemical analyses show that the  $\text{Co}_3(\text{PO}_4)_2$  nanosphere-modified electrode exhibited an admirable electrocatalytic activity for the oxidation of methanol in alkaline media. An extended investigation was made for the methanol oxidation by varying the experimental reaction parameters, such as catalyst loading, methanol concentration, and long-term stability for electro-oxidation of methanol. The superior electrocatalytic activity of  $\text{Co}_3(\text{PO}_4)_2$  should be attributed to its good surface morphological structure and high number of active surface sites. These results demonstrate that the  $\text{Co}_3(\text{PO}_4)_2$  nanospheres could be one a low-cost, more abundant, and a competent electrocatalyst for direct methanol fuel cells.

**Acknowledgments:** The authors would like to extend their sincere appreciation to the Deanship of Scientific Research at King Saud University for funding this research group NO: RG-1438-001.

**Author Contributions:** Prabhakarn Arunachalam performed the experiments and wrote the manuscript. Abdullah Salah Alamoudi, Mohamed A. Ghanem, and Abdullah M. Al-Mayouf provided suggestions and assistance in experiment design and manuscript editing. Maged N. Shaddad assisted in experimental work.

**Conflicts of Interest:** The authors declare no conflict of interest.

## References

1. Peng, L.; Gan, L.; Wei, Y.; Yang, H.; Li, J.; Du, H.; Kang, F. Pt submonolayers on Au nanoparticles: coverage-dependent atomic structures and electrocatalytic stability on methanol oxidation. *J. Phys. Chem. C* **2016**, *120*, 28664–28671. [[CrossRef](#)]
2. Arunachalam, P.; Zhang, S.; Abe, T.; Komura, M.; Iyoda, T.; Nagai, K. Weak visible light (~mW/cm<sup>2</sup>) organophotocatalysis for mineralization of amine, thiol and aldehyde by biphasic cobalt phthalocyanine/fullerene nanocomposites prepared by wet process. *Appl. Catal. B* **2016**, *193*, 240–247. [[CrossRef](#)]
3. Puthiyapura, V.K.; Brett, D.J.L.; Russell, A.E.; Lin, W.F.; Hardacre, C. Biobutanol as fuel for direct alcohol fuel cells—Investigation of Sn-modified Pt catalyst for butanol electro-oxidation. *ACS Appl. Mater. Interfaces* **2016**, *8*, 12859–12870. [[CrossRef](#)] [[PubMed](#)]
4. Prathap, M.U.A.; Satpati, B.; Srivastava, R. Facile preparation of  $\beta$ -Ni(OH)<sub>2</sub>-NiCo<sub>2</sub>O<sub>4</sub> hybrid nanostructure and its application in the electro-catalytic oxidation of methanol. *Electrochim. Acta* **2014**, *130*, 368–380. [[CrossRef](#)]
5. Noroozifar, M.; Yavari, Z.; Motlagh, M.K.; Ghasemi, T.; Yazdi, S.H.R.; Mohammadi, M. Fabrication and performance evaluation of a novel membrane electrode assembly for DMFCs. *RSC Adv.* **2016**, *6*, 563–574. [[CrossRef](#)]
6. Tong, Y.Y.; Gu, C.D.; Zhang, J.L.; Tang, H.; Li, Y.; Wang, X.L.; Tu, J.P. Urchin-like Ni-Co-P-O nanocomposite as novel methanol electro-oxidation materials in alkaline environment. *Electrochim. Acta* **2016**, *187*, 11–19. [[CrossRef](#)]
7. Ghanem, M.A.; Al-Mayouf, A.M.; Arunachalam, P.; Abiti, T. Mesoporous cobalt hydroxide prepared using liquid crystal template for efficient oxygen evolution in alkaline media. *Electrochim. Acta* **2016**, *207*, 177–186. [[CrossRef](#)]
8. Atar, N.; Eren, T.; Yola, M.L.; Karimi-Maleh, H.; Demirdögen, B. Magnetic iron oxide and iron oxide@gold nanoparticle anchored nitrogen and sulfur-functionalized reduced graphene oxide electrocatalyst for methanol oxidation. *RSC Adv.* **2015**, *5*, 26402–26409. [[CrossRef](#)]
9. Arunachalam, P.; Ghanem, M.A.; Al-Mayouf, A.M.; Al-shalwi, M.; Abd-Elkader, O.H. Microwave assisted synthesis and characterization of Ni/NiO nanoparticles as electrocatalyst for methanol oxidation in alkaline solution. *Mater. Res. Express* **2017**, *4*, 025035. [[CrossRef](#)]
10. Sun, J.; Dou, M.; Zhang, Z.; Ji, J.; Wang, F. Carbon nanotubes supported Pt-Co-P ultrafine nanoparticle electrocatalysts with superior activity and stability for methanol electro-oxidation. *Electrochim. Acta* **2016**, *215*, 447–454. [[CrossRef](#)]
11. Gao, M.R.; Gao, Q.; Jiang, J.; Cui, C.H.; Yao, W.T.; Yu, S.H. A methanol-tolerant Pt/CoSe<sub>2</sub> nanobelt cathode catalyst for direct methanol fuel cells. *Angew. Chem.* **2011**, *123*, 5007–5010. [[CrossRef](#)]
12. Shi, M.; Zhang, W.; Li, Y.; Chu, Y.; Ma, C. Tungsten carbide-reduced graphene oxide intercalation compound as co-catalyst for methanol oxidation. *Chin. J. Catal.* **2016**, *37*, 1851–1859. [[CrossRef](#)]
13. Cui, P.; He, H.; Liu, H.; Zhang, S.; Yang, J. Heterogeneous nanocomposites of silver selenide and hollow platinum nanoparticles toward methanol oxidation reaction. *J. Power Sources* **2016**, *327*, 432–437. [[CrossRef](#)]
14. Yang, C.; Srinivasan, S.; Aricò, A.S.; Creti, P.; Baglio, V.; Antonucci, V. Composite nafion/zirconium phosphate membranes for direct methanol fuel cell operation at high temperature. *Electrochem. Solid-State Lett.* **2001**, *4*, A31–A34. [[CrossRef](#)]
15. Tan, J.; Yang, J.H.; Liu, X.; Yang, F.; Li, X.; Ma, D. Electrochemical oxidation of methanol on mesoporous nickel phosphates and Si-incorporated mesoporous nickel phosphates. *Electrochem. Commun.* **2013**, *27*, 141–143. [[CrossRef](#)]
16. Kiyani, R.; Rowshanzamir, S.; Parnian, M.J. Nitrogen doped graphene supported palladium-cobalt as a promising catalyst for methanol oxidation reaction: Synthesis, characterization and electrocatalytic performance. *Energy* **2016**, *113*, 1162–1173. [[CrossRef](#)]
17. Kepeniene, V.; Tamasiunait, L.T.; Jablonskiene, J.; Semasko, M.; Vaiciunien, J.; Vaitkus, R.; Norkus, E. One-pot synthesis of graphene supported platinum cobalt nanoparticles as electrocatalysts for methanol oxidation. *Mater. Chem. Phys.* **2016**, *171*, 145–152. [[CrossRef](#)]
18. Poon, K.C.; Khezri, B.; Li, Y.; Webster, R.D.; Suc, H.; Sato, H. A highly active Pd-P nanoparticle electrocatalyst for enhanced formic acid oxidation synthesized via stepwise electroless deposition. *Chem. Commun.* **2016**, *52*, 3556–3559. [[CrossRef](#)] [[PubMed](#)]

19. Tan, D.C.L.; Khezri, B.; Amatyakul, W.; Webster, R.D.; Sato, H. A facile synthesized highly active Pd nanoparticle electrocatalyst for electroless deposition process. *RSC Adv.* **2015**, *5*, 88805–88808. [[CrossRef](#)]
20. Li, T.; Fu, G.; Su, J.; Wang, Y.; Lv, Y.; Zou, X.; Zhu, X.; Xu, L.; Sun, D.; Tang, Y. Carbon supported ultrafine gold phosphorus nanoparticles as highly efficient electrocatalyst for alkaline ethanol oxidation reaction. *Electrochim. Acta* **2017**, *231*, 13–19. [[CrossRef](#)]
21. Poon, K.C.; Tan, D.C.L.; Vo, T.D.T.; Khezri, B.; Su, H.; Webster, R.D.; Sato, H. Newly developed stepwise electroless deposition enables a remarkably facile synthesis of highly active and stable amorphous Pd nanoparticle electrocatalysts for oxygen reduction reaction. *J. Am. Chem. Soc.* **2014**, *136*, 5217–5220. [[CrossRef](#)] [[PubMed](#)]
22. Zhang, K.; Wang, C.; Bin, D.; Wang, J.; Yan, B.; Shiraiishi, Y.; Du, Y. Fabrication of Pd/P nanoparticle networks with high activity for methanol oxidation. *Catal. Sci. Technol.* **2016**, *6*, 6441–6447. [[CrossRef](#)]
23. Zhang, M.; Yan, Z.; Li, Y.; Jing, J.; Xie, J. Preparation of cobalt silicide on graphene as Pt electrocatalyst supports for highly efficient and stable methanol oxidation in acidic media. *Electrochim. Acta* **2015**, *161*, 48–54. [[CrossRef](#)]
24. Theerthagiri, J.; Thiagarajan, K.; Senthilkumar, B.; Khan, Z.; Senthil, R.A.; Arunachalam, P.; Madhavan, J.; Ashokkumar, M. Synthesis of hierarchical cobalt phosphate nanoflakes and their enhanced electrochemical performances for supercapacitor applications. *ChemistrySelect* **2016**, *1*, 1–11. [[CrossRef](#)]
25. Combes, C.; Rey, C. Amorphous calcium phosphates: Synthesis, properties and uses in biomaterials. *Acta Biomater.* **2010**, *6*, 3362–3378. [[CrossRef](#)] [[PubMed](#)]
26. Kim, K.H.; Jeong, J.M.; Lee, S.J.; Choi, B.G.; Lee, K.G. Protein-directed assembly of cobalt phosphate hybrid nanoflowers. *J. Colloid Interface Sci.* **2016**, *484*, 44–50. [[CrossRef](#)] [[PubMed](#)]
27. Theerthagiri, J.; Senthil, R.A.; Buraidah, M.H.; Raghavender, M.; Madhavan, J.; Arof, A.K. Synthesis and characterization of  $(\text{Ni}_{1-x}\text{Co}_x)\text{Se}_2$  based ternary selenides as electrocatalyst for triiodide reduction in dye-sensitized solar cells. *J. Solid State Chem.* **2016**, *238*, 113–120. [[CrossRef](#)]
28. Arunachalam, P.; Ghanem, M.A.; Al-Mayouf, A.M.; Al-shalwi, M. Enhanced electrocatalytic performance of mesoporous nickel-cobalt oxide electrode for methanol oxidation in alkaline solution. *Mater. Lett.* **2017**, *196*, 365–368. [[CrossRef](#)]
29. Al-Enizia, A.M.; Ghanem, M.A.; El-Zatahry, A.A.; Al-Deyab, S.S. Nickel oxide/nitrogen doped carbon nanofibers catalyst for methanol oxidation in alkaline media. *Electrochim. Acta* **2014**, *137*, 774–780. [[CrossRef](#)]
30. Hameed, R.M.A.; El-Khatib, K.M. Ni-P and Ni-Cu-P modified carbon catalysts for methanol electro-oxidation in KOH solution. *Int. J. Hydrog. Energy* **2010**, *35*, 2517–2529. [[CrossRef](#)]
31. Xu, C.; Cheng, L.; Shen, P.; Liu, Y. Methanol and ethanol electrooxidation on Pt and Pd supported on carbon microspheres in alkaline media. *Electrochem. Commun.* **2007**, *9*, 997–1001. [[CrossRef](#)]
32. Asgari, M.; Maragheh, M.G.; Davarkhah, R.; Lohrasbi, E. Methanol electrooxidation on the nickel oxide nanoparticles/multi-walled carbon nanotubes modified glassy carbon electrode prepared using pulsed electrodeposition. *J. Electrochem. Soc.* **2011**, *158*, K225–K229. [[CrossRef](#)]
33. Barakat, N.A.M.; El-Newehy, M.; Al-Deyab, S.S.; Kim, H.Y. Cobalt/copper-decorated carbon nanofibers as novel non-precious electrocatalyst for methanol electrooxidation. *Nanoscale Res. Lett.* **2014**, *9*, 2. [[CrossRef](#)] [[PubMed](#)]
34. Huang, W.; Wang, H.; Zhou, J.; Wang, J.; Duchesne, P.N.; Muir, D.; Zhang, P.; Han, N.; Zhao, F.; Zeng, M.; et al. Highly active and durable methanol oxidation electrocatalyst based on the synergy of platinum–nickel hydroxide–grapheme. *Nat. Commun.* **2015**, *6*, 10035. [[CrossRef](#)] [[PubMed](#)]

